ISBN number: 978-1-925627-66-4

Normal Paper ☒
Student Paper ☐
Young Engineer Paper ☐

Photonic integrated circuit compatible interrogation methods for low SWaP optical fibre strain sensing

Luke H. Broadley[1], Andreas Boes[1,2], Joel Smithard[3], Cedric Rosalie[3], Suzana Turk[3], Nik Rajic[3], Pier Marzocca[4], and Arnan Mitchell[1]

[1] *Integrated Photonics and Applications Centre, RMIT University, Melbourne, Australia*
[2] *School of Electrical and Electronic Engineering, University of Adelaide, Adelaide, Australia*
[3] *Defence Science and Technology Group, 506 Lorimer Street, Fishermans Bend, Australia*
[4] *Sir Lawrence Wackett Defence and Aerospace Centre, RMIT University, Melbourne, Australia*

Abstract

Optical fibre strain sensors are high performance, durable, lightweight, and require relatively low power, however the systems that are used to interrogate these sensors are typically heavy and bulky, largely negating the advantages of optical fibre strain sensing in situations where low size, weight, and power (SWaP) is required. This project looks at addressing the SWaP concerns of optical fibre interrogation systems via photonic integrated circuit (PIC) compatible interrogation methods. Using bulk optical components, the use of the Pound-Drever-Hall (PDH) laser frequency locking technique as a PIC compatible means to interrogate optical fibre strain sensors is investigated. This proof of concept paves the way to developing ultra-low SWaP interrogators that can be of the size of a fingernail, leading to new possibilities in strain sensing.

Keywords: SWaP, optical fibre sensors, photonic integrated circuits, Pound-Drever-Hall, strain sensing, structural health monitoring.

Introduction

Traditional optical fibre strain sensors use fibre Bragg gratings (FBGs) as wavelength selective mirrors. As strain is applied to the FBG, the reflected wavelength shifts; it is this shift that is monitored as a strain signal. Such optical fiber strain sensors offer many advantages over conventional electro-mechanical sensing technologies such as improved sensitivity, immunity to electromagnetic interference, and form factor [1]. However, in low SWaP requirement scenarios, such as structural health monitoring (SHM), the size and power requirements of the bulk optical interrogators can largely negate the advantages of optical fibre strain sensing systems, limiting their practical use.

Photonic integrated circuits (PICs) have progressed tremendously in the last decade; indeed, it is now possible to integrate many bulk optical components such as lasers, modulators, and detectors all on a single chip [2]. The ability to miniaturise the bulk optical components of the interrogation system onto a single integrated circuit the size of a fingernail will enable the advancement of SHM applications that previously were thought of as too complex. However, so far, progress in using PICs as interrogators for SHM applications is limited, in part due to the complexity of integrating the full complement of optical components required for the interrogation system onto a single PIC.

One such PIC compatible method to interrogate optical sensors is the PDH laser frequency locking technique, which has traditionally been used to stabilise lasers to external cavities. Laser frequency locking has been employed in extremely sensitive instruments, such as the Laser Interferometer Gravitational Wave Observatory (LIGO) [3], while also seeing use in optical fibre sensing scenarios [4]. In the case of optical strain sensing, Fabry-Perot cavities, made with a matched pair of fibre Bragg gratings (FP-FBG), were initially used as the sensing element, with the PDH technique being used to lock onto the resonant features in the reflected beam [5]. Ultrahigh resolution strain measurements in the range of fϵ (femto-strain), along with micro-Kelvin temperature sensing resolution have been demonstrated [6], while dynamic strain signals can range from less than 1 Hz to near 6 MHz ultrasonic signals using the same sensing element [7]. Along with FP-FBGs, recent work has gone into using π-phase shifted FBGs (πPS-FBG) as the sensing element for PDH measurements [8,9]. πPS-FBGs are a single FBG with a half-period, π, shift at the centre of the FBG to create a single resonance Fabry-Perot cavity. Using πPS-FBGs as the sensing element has the advantage of a smaller sensor footprint, as a single FBG is used to create the resonance response required for PDH locking; in contrast, two FBGs separated by some distance is required for FP-FBG sensing elements. Quasi-static πPS-FBGs strain sensors have been shown to reach sub nano-strain levels [10] while ultrasonic sensing can be undertaken at frequencies up to 200 kHz [11].

RMIT and DSTG are investigating the use of the PDH frequency locking technique as a PIC compatible interrogation method for optical fibre strain sensors. The authors show that using bulk optical components, it is possible to recover static strain signals with a sensitivity in the order of hundreds of nϵ (nano-strain) using both FP-FBG and πPS-FBG sensing elements. Ultrasonic strain signals, up to 2 MHz, are shown to be recovered using the πPS-FBG as the sensing element. The ability to decouple the static/quasi-static strain signals from dynamic signals in hardware through laser tuning, using a signal sensing element is also demonstrated.

Background

Pound-Drever-Hall as an interrogation method

Figure 1(a) presents the schematic for a typical PDH system. A tunable laser (MOGLabs CES), with frequency, ω, is phase modulated by a local oscillator (LO) at some frequency, ϕ, generating two sidebands at $\omega \pm \phi$. This modulated signal is fed into an optical circulator and is then incident on the optical fibre sensing element, in this case either a FP-FBG or πPS-FBG.

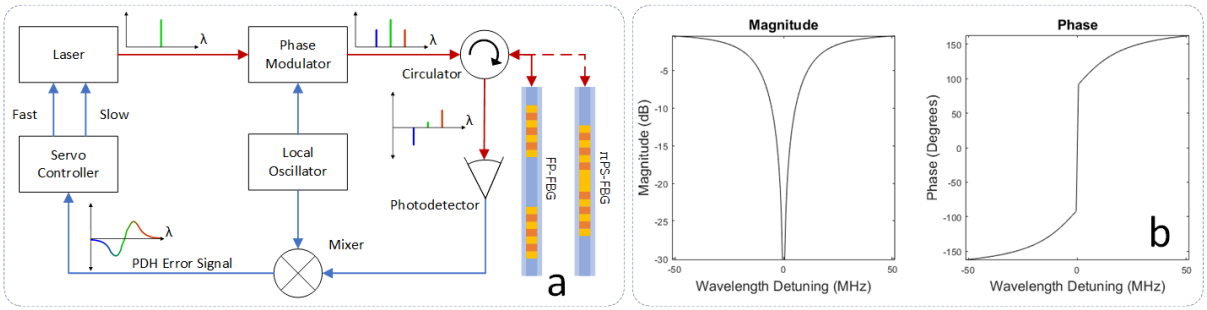

Fig. 1: (a) Simplified block diagram of the PDH technique used as an optical interrogator of a FP-FBG sensing element. (b) Complex reflective transfer function for FP-FBG.

The cavity in the sensing element creates conditions where the incident light forms resonant modes; the complex transfer function of these resonant modes for a FP-FBG element with a 10 mm cavity is presented in Fig. 1(b). At these resonant wavelengths, the incident laser light passes through the sensing element, causing the reflected light to be at a minimum. If the sensing element is stretched or compressed (or experiences a thermal change), the resonant wavelength will change, causing the reflected power at the incident laser wavelength, ω, to increase (Magnitude plot, Fig. 1(b)). This increase in power does not, however, provide enough

information to conclude if the sensing element was stretched or compressed as the reflected magnitude of the resonant mode is symmetric. To identify if the laser frequency is above or below the cavity resonance, the phase of the resonant mode (Phase plot, Fig. 2(b)) must be measured. As the laser is phase modulated at the LO frequency, ϕ, the sidebands at $\omega \pm \phi$ will sample the phase of the cavity resonance at either side of the laser frequency. The three reflected beams, the laser and two sidebands, are interfered at the photodetector and the sum will beat at the LO frequency. The phase of the beat signal is directly related to the phase of the cavity's resonant mode. This beat signal, now in the electrical domain, is homodyne mixed with the LO to generate what is called the PDH error signal, which has a zero crossing at resonance much like the phase response of the cavity. The error signal is fed into a servo controller (MOGLabs FSC) which is used to lock the tunable laser to a resonance by tracking the zero crossing and compensating the wavelength accordingly. It is this electronic signal from the servo controller to the tunable laser that is tapped and used to measure the strain.

Mechanical experimental setup

The purpose of this work is to investigate the use of the PDH technique as a means of strain sensing for the static/quasi-static and ultrasonic regimes in the context of SHM. The low frequency signals represent static/quasi-static loads, such as take-off or manoeuvre loads in an aircraft wing, or temperature changes, e.g., induced by a change in aircraft altitude. The dynamic/ultrasonic signals being interrogated can arise due to impacts on a wing via e.g., hailstone or bird strike, and normally consist of Lamb waves. Modal decomposition of these Lamb waves can potentially be used to identify, localise, and characterise the impact.

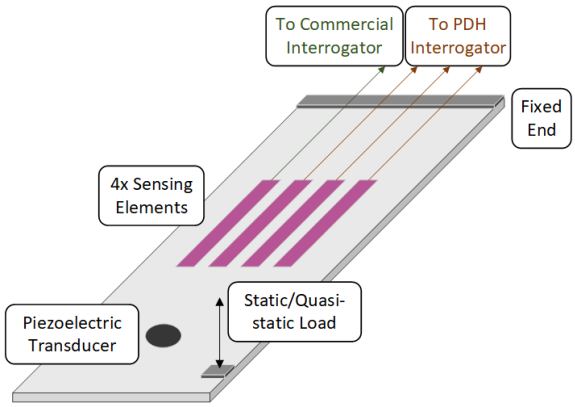

Fig. 2: Schematic of experimental setup for static/quasi-static and dynamic strain measurements

Figure 2 shows a schematic of the experimental setup used to apply strain loads under static conditions through to ultrasonic frequencies on an aluminium coupon. The coupon is fixed at one end, creating a cantilever beam with dimensions 400×46×3 mm (l×w×t). Four sensing elements were bonded to the beam: 1× FBG (for benchmarking with a commercial FBG interrogator), 2×FP-FBGs with 10 mm and 20 mm cavity lengths, and 1×πPS-FBG. Weights were added to the moving end of the cantilever for the static load measurements with a variable speed motor used for further static load and quasi-static load measurements. Dynamic measurements, above 50 kHz, were achieved using a 10 mm diameter piezoelectric transducer bonded to the cantilever. The piezoelectric transducer is driven by the AUSAM+ unit [12] and excites acoustic waves in the coupon via a 5-cycle, Hanning windowed, sinusoidal burst of up to 200 $V_{p\text{-}p}$.

The PDH interrogation system is locked to either the 10 mm FP-FBG or the πPS-FBG for the following results. The calibration from servo voltage to a strain value is accomplished by comparing a commercial interrogator (SmartScan Aero Mini) read-out from a standard FBG with the results from the PDH interrogation, of either a FP-FBG or the πPS-FBG. A quasi-static load is applied to determine a scaling factor for conversion. This is a first order calibration, as the derived scaling factor is wavelength (optical) independent, and one should consider that the gain of the servo controller and the output servo voltage, are dependent on both the wavelength

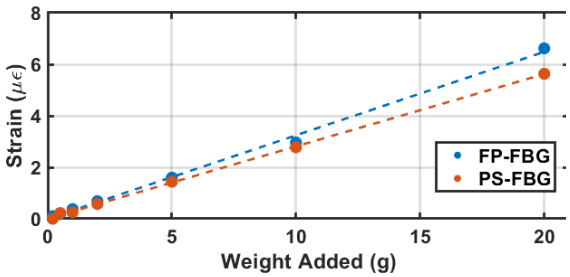

Fig. 3: Static strain measurements for 10mm FP-FBG and πPS-FBG.

of the laser as well as the acoustic frequency of input (strain) signal. As a result, the strain values presented in the following analysis are only representative.

Results and Discussion

Static measurements

Using the setups in Fig. 1(a) and Fig. 2 with the 10 mm FP-FBG and πPS-FBG as the sensing elements, the cantilever was loaded with increasing amounts of weight and the strain measured using the PDH interrogator. Fig. 3, shows that FP-FBG sees a larger strain than the πPS-FBG for the same load. This increase may be due to the larger sensing area of the FP-FBG (10 mm) than that of the πPS-FBG (~2 μm), leading to the FP-FBG sampling the strain across a larger area. The dynamic range of the static measurements is limited to approximately 15 με (micro-strain) due to the limited mode-hop-free wavelength tuning range of the external cavity tunable laser used.

Dynamic measurements

For the dynamic strain signal measurements, the transducer was activated with a 50 $V_{p\text{-}p}$ sinusoidal burst at a 2 MHz centre frequency, exciting Lamb waves within the aluminium coupon. Fig. 4(a) shows the recovered strain signal when using the 10 mm FP-FBG with Fig. 4(b) showing the recovered strain for the πPS-FBG. The peak strain for the FP-FBG shows an approximate 5-fold increase in measured strain when compared to the πPS-FBG.

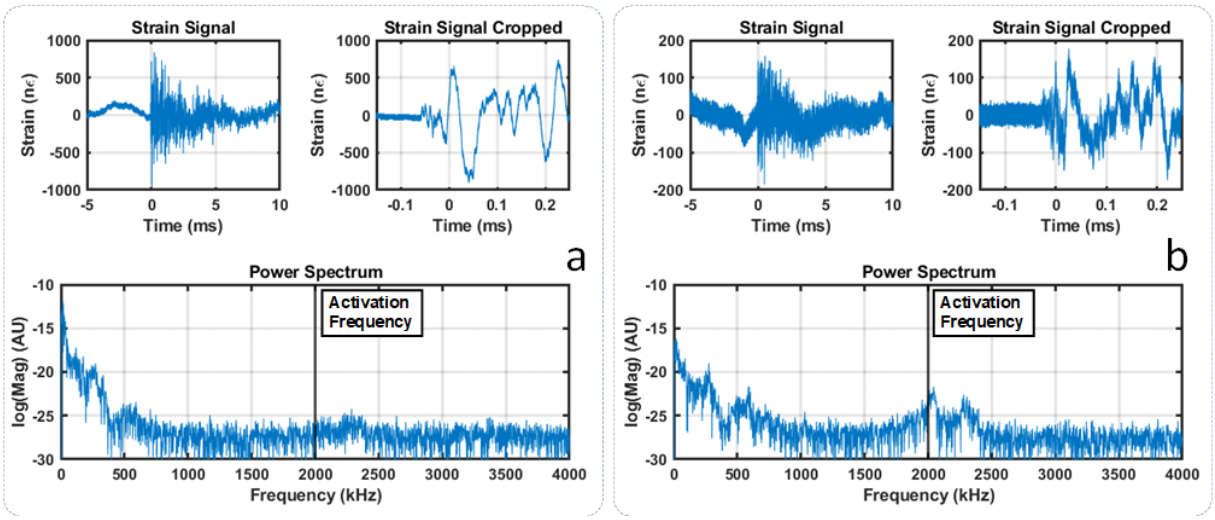

Fig. 4: Recovered 2 MHz acoustic Lamb wave on aluminium coupon using PDH interrogation method with (a) 10 mm FP-FBG and (b) πPS-FBG as the sensing elements.

The two power spectrums presented in Fig. 4 show that the πPS-FBG can successfully recover the 2 MHz signal from the transducer whereas the FP-FBG is unable to. This may be due to the wavelength of the acoustic waves in the aluminium coupon at a 2 MHz activation being between 1.8 and 3.5 mm, meaning that several acoustic waves would be measured within the 10 mm sensing area of the FP-FBG, averaging the signal. Comparing the "Strain Signal Cropped" plots in Figs. 4(a) and 4(b), it can be seen that the higher frequencies are not visible for the FP-FBG (Fig. 4(a)). It appears that the large sensing area is acting as a low pass filter, with the sensor only able to recover the larger bulk changes in strain across the sensing element.

Hardware decoupling of static and dynamic measurements

The tunable laser used in this experiment has two independent mechanisms of tuning the output wavelength. A piezoelectric actuator within the laser is used to physically change the round-trip length within the external cavity of the laser, tuning the wavelength. The laser diode injection current can also be used to tune the output wavelength independently of the actuator tuning. The servo controller used in this experiment can output two independent control signals, fast and slow as depicted in Fig. 1(a), to the tunable laser. These two signals control the two tuning mechanisms with the slow signal controlling the actuator and the fast signal controlling the injection current. This allows for the decoupling of the static/quasi-static signal from the dynamic signals to happen in hardware. The theoretical bandwidth for these two signals ranges from DC to 10 MHz and is limited by the tunable laser and servo controller.

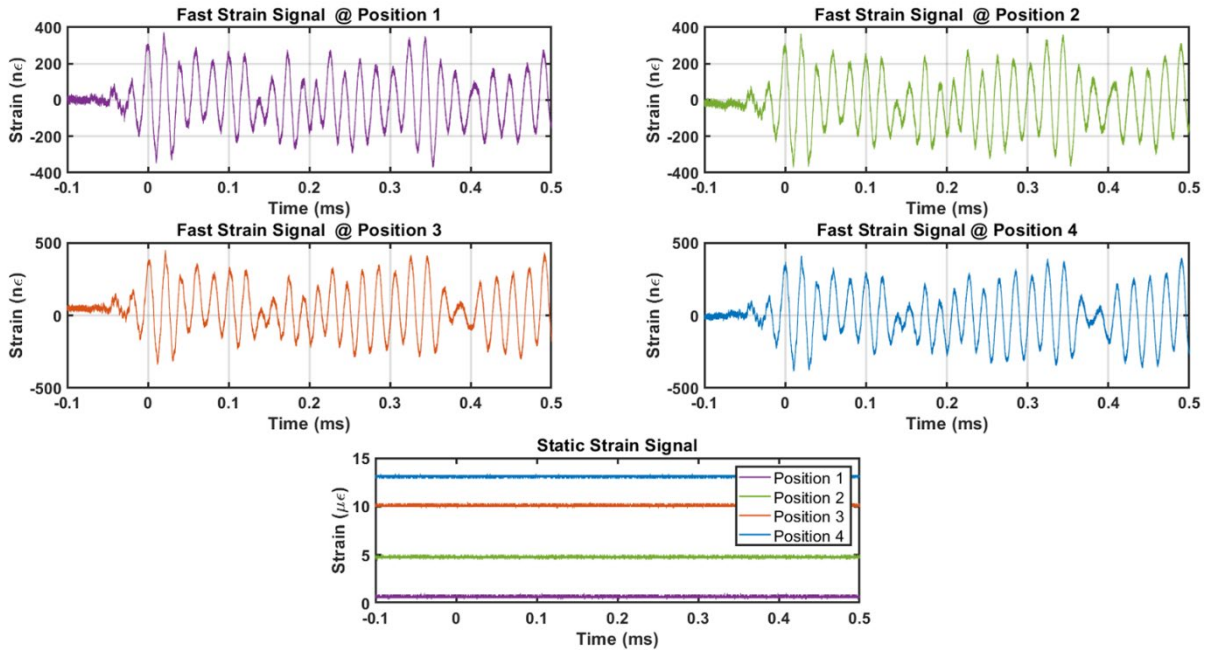

Fig. 5: Decoupling of static and dynamic measurements of a single πPS-FBG sensing element using single laser source.

To explore this decoupling, different static loads were applied to the coupon using the external motor while simultaneously activating dynamic signals with the piezoelectric transducer at 50 kHz and 50 $V_{p\text{-}p}$. Fig. 5 shows the results of the decoupling with four static loads from 1 με to 13 με with the relative recovered dynamic signals when using the πPS-FBG. It can be seen that as the static load is increased, the dynamic signals remain centered around zero, showing the successful decoupling. With the increase in static load, the envelope of the dynamic measurements changes as the propagation of the acoustic waves is altered. This is particularly evident at approximately 0.4 ms.

Benefits of photonic integration

The PDH interrogation method was chosen initially as a PIC compatible technique, with the possibility of integrating the tunable laser, phase modulator, circulator, and photodetector all onto a single PIC the size of a fingernail. In addition to significantly reducing the SWaP of the optical readout system, integrated lasers have the benefit of having large mode-hop-free tuning ranges that can be of the order of tens of nanometres, increasing the dynamic range by approximately three orders of magnitude, with a theoretical dynamic range of the order of tens of mϵ (milli-strain). Integrated tunable lasers are also able to decouple the static/quasi-static signals from the dynamic signals via multiple wavelength tuning mechanisms. The static/quasi-static signals can be compensated for using integrated heaters that change the cavity length of the laser with bandwidths from DC to tens of kHz achievable [13]. The dynamic measurements

can be compensated by exploiting the electro-optic effect of certain PIC media, such as Lithium Niobate on insulator, with bandwidths in excess of 100 GHz possible [14].

Conclusion

Using bulk optical components, the authors demonstrate that the PDH frequency locking technique can be used as a PIC compatible interrogation method for optical strain sensors in the context of SHM. Static loads and dynamic strain signals, up to 2 MHz, were recovered using a πPS-FBG as the sensing element. Hardware decoupling of static/quasi-static signals from dynamic signals is possible using this method with limited dynamic range as a result of the bulk tunable laser. A discussion about PICs and integration was provided, showing a number of potential benefits over bulk systems such as extremely low SWaP and improvements in dynamic range.

Acknowledgments

The authors would like to thank MOGLabs for support during the initial Pound-Drever-Hall experimental setup phase.

References

[1] Yin, S., Ruffin, P. B., and Yu, F. T. S. *Fiber Optic Sensors*. 2008.

[2] Thomson, D., Zilkie, A., Bowers, J. E., Komljenovic, T., Reed, G. T., Vivien, L., Marris-Morini, D., Cassan, E., Virot, L., Fédéli, J.-M., Hartmann, J.-M., Schmid, J. H., Xu, D.-X., Boeuf, F., O'Brien, P., Mashanovich, G. Z., and Nedeljkovic, M. "Roadmap on Silicon Photonics." *Journal of Optics*, Vol. 18, No. 7, 2016, p. 073003. https://doi.org/10.1088/2040-8978/18/7/073003.

[3] Black, E. D. "An Introduction to Pound–Drever–Hall Laser Frequency Stabilization." *American Journal of Physics*, Vol. 69, No. 1, 2001, pp. 79–87. https://doi.org/10.1119/1.1286663.

[4] Liu, Q., Zhao, S., and He, Z. "Improved Pound-Drever-Hall Techniques for High Resolution Optical Fiber Grating Sensors." *Journal of Lightwave Technology*, Vol. 14, No. 8, 2021, pp. 1–1. https://doi.org/10.1109/JLT.2021.3052170.

[5] Chow, J. H., McClelland, D. E., Gray, M. B., and Littler, I. C. M. "Demonstration of a Passive Subpicostrain Fiber Strain Sensor." *Optics Letters*, Vol. 30, No. 15, 2005, p. 1923. https://doi.org/10.1364/OL.30.001923.

[6] Zhao, S., Liu, Q., Chen, J., and He, Z. "Resonant Fiber-Optic Strain and Temperature Sensor Achieving Thermal-Noise-Limit Resolution." *Optics Express*, Vol. 29, No. 2, 2021, p. 1870. https://doi.org/10.1364/OE.415611.

[7] Barnes, J., Li, S., Goyal, A., Abolmaesumi, P., Mousavi, P., and Loock, H.-P. "Broadband Vibration Detection in Tissue Phantoms Using a Fiber Fabry–Perot Cavity." *IEEE Transactions on Biomedical Engineering*, Vol. 65, No. 4, 2018, pp. 921–927. https://doi.org/10.1109/TBME.2017.2731663.

[8] Gatti, D., Galzerano, G., Janner, D., Longhi, S., and Laporta, P. "Fiber Strain Sensor Based on a π-Phase-Shifted Bragg Grating and the Pound-Drever-Hall Technique." *Optics Express*, Vol. 16, No. 3, 2008, p. 1945. https://doi.org/10.1364/OE.16.001945.

[9] Chen, J., Liu, Q., and He, Z. "High-Resolution Simultaneous Measurement of Strain and Temperature Using π-Phase-Shifted FBG in Polarization Maintaining Fiber." *Journal of Lightwave Technology*, Vol. 35, No. 22, 2017, pp. 4838–4844. https://doi.org/10.1109/JLT.2017.2760343.

[10] Chen, J., Liu, Q., Fan, X., and He, Z. "Ultrahigh Resolution Optical Fiber Strain Sensor Using Dual Pound–Drever–Hall Feedback Loops." *Optics Letters*, Vol. 41, No. 5, 2016, p. 1066. https://doi.org/10.1364/OL.41.001066.

[11] Guo, J., and Yang, C. "Highly Stabilized Phase-Shifted Fiber Bragg Grating Sensing System for Ultrasonic Detection." *IEEE Photonics Technology Letters*, Vol. 27, No. 8, 2015, pp. 848–851. https://doi.org/10.1109/LPT.2015.2396530.

[12] Smithard, J., Rajic, N., van der Velden, S., Norman, P., Rosalie, C., Galea, S., Mei, H., Lin, B., and Giurgiutiu, V. "An Advanced Multi-Sensor Acousto-Ultrasonic Atructural Health Monitoring System Development and Aerospace Demonstration." *Materials*, Vol. 10, No. 7, 2017, p. 832. https://doi.org/10.3390/ma10070832.

[13] Xiao, H., Zhang, Z., Yang, J., Han, X., Chen, W., Ren, G., Mitchell, A., Yang, J., Gao, D., and Tian, Y. "On-Chip Scalable Mode-Selective Converter Based on Asymmetrical Micro-Racetrack Resonators." *Nanophotonics*, Vol. 9, No. 6, 2020, pp. 1447–1455. https://doi.org/10.1515/nanoph-2020-0040.

[14] Mercante, A. J., Yao, P., Shi, S., Schneider, G., Murakowski, J., and Prather, D. W. "110 GHz CMOS Compatible Thin Film LiNbO3 Modulator on Silicon." *Optics Express*, Vol. 24, No. 14, 2016, p. 15590. https://doi.org/10.1364/OE.24.015590.